ACS Synthetic Biology

Letter

Cite This: ACS Synth. Biol. 2020, 9, 19−25

pubs.acs.org/synthbio

Design of Mammalian ON-Riboswitches Based on Tandemly Fused Aptamer and Ribozyme

Kamila Mustafina, Keisuke Fukunaga, and Yohei Yokobayashi*

Nucleic Acid Chemistry and Engineering Unit, Okinawa Institute of Science and Technology Graduate University, Onna, Okinawa 904 0495, Japan

Supporting Information

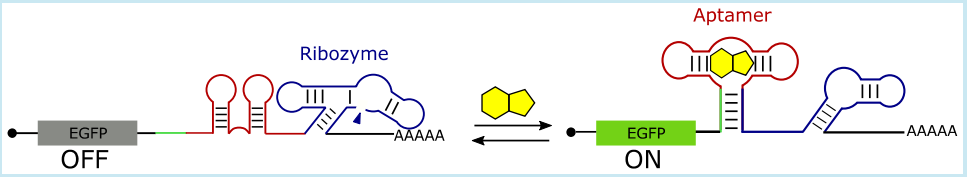

ABSTRACT: Self-cleaving ribozymes engineered to be activated or inhibited by a small molecule binding to an RNA aptamer inserted within a ribozyme (aptazymes) have proven to be useful for controlling gene expression in living cells. In mammalian cells, an aptazyme embedded in the 5′ or 3′ untranslated region of an mRNA functions as a synthetic riboswitch to chemically regulate gene expression. However, the variety of aptazyme architectures and the ribozyme scaffolds that have been used for mammalian riboswitches has been limited. In particular, fewer synthetic riboswitches that activate gene expression in response to a small molecule (ON-switches) in mammalian cells have been reported compared to OFF-switches. In this work, we developed mammalian riboswitches that function as guanine-activated ON-switches based on a novel aptazyme architecture in which an aptamer and a ribozyme are fused in tandem. The riboswitch performance was optimized by fine-tuning the stability of a critical stem that controls the ribozyme structure and function, yielding switches with ON/OFF ratios greater than 6.0. Our new aptazyme architecture expands the RNA device toolbox for controlling gene expression in mammalian cells.

KEYWORDS: *RNA engineering, twister ribozyme, aptamer, aptazyme, riboswitch*

Synthetic riboswitches enable chemical regulation of gene expression without engineered proteins. An aptamer, or a short segment of RNA that specifically binds its target molecule, acts as a chemical sensor, and various mechanisms are used to couple aptamer-target binding with gene expression at the RNA level.[1−4] In mammalian cells, insertion of one or more allosterically controlled ribozymes, or aptazymes, in the 5′ or 3′ untranslated region (UTR) of the mRNA of the gene to be regulated is a well-established strategy to regulate gene expression by a small molecule.[5] The aptazyme consists of a self-cleaving ribozyme and an aptamer designed so that self-cleavage is either activated or inhibited by a small molecule that binds to the aptamer. Ribozyme cleavage within the UTR of an mRNA results in diminished gene expression (OFF), whereas ribozyme inhibition upregulates the encoded protein expression (ON).

These self-cleaving aptazymes represent compact, *cis*-acting, and portable RNA devices to control gene expression in mammalian cells. Recent applications of aptazyme-based riboswitches in mammalian cells and animals include chemical regulation of T-cell proliferation,[6] and controlling viral replication and viral gene expression.[7−12] However, the variety of aptazymes that have been experimentally demonstrated in mammalian cells remains limited. Aptazymes are typically designed by inserting an aptamer within a stem loop of a ribozyme, and by optimizing the "communication module" that bridges the two RNA elements *via* extensive screening or design-build-test cycles.[6,12−16] To date, only the hammerhead and the hepatitis delta virus (HDV) ribozymes have been used to engineer riboswitches in mammalian cells. Interestingly, OFF-switches (downregulation of gene expression in response to a small molecule) are more common,[12−15,17] whereas only a few aptazyme-based ON-switches have been reported in mammalian cells.[6,16,18,19]

We recently described a novel architecture for small molecule-inhibited aptazymes.[20] Instead of inserting an aptamer within a stem loop of a ribozyme, an aptamer and a ribozyme were fused in tandem. Furthermore, an antiribozyme (anti-Rz) sequence was inserted upstream of the aptamer which is partially complementary to the ribozyme sequence (Figure 1). In this design, the aptazyme can adopt either the ribozyme (*Rz*) or the aptamer (*Apt*) structure. The two structures are exclusive, and only the *Rz* structure results in self-cleavage (gene expression OFF). The base stem of the ribozyme P_{rz} is an essential structural element of the ribozyme. Similarly, formation of P_{apt}, the base stem of the aptamer which includes the 5′ side of P_{rz}, is also critical for ligand binding (Figure 1). It is expected that if P_{apt} is too stable, the aptazyme assumes the *Apt* structure; therefore, gene expression is ON. If P_{apt} is too unstable, and therefore P_{rz} is too stable, the aptazyme forms the *Rz* structure resulting in low gene

Received: September 12, 2019
Published: December 10, 2019

DOI: 10.1021/acssynbio.9b00371
ACS Synth. Biol. 2020, 9, 19−25

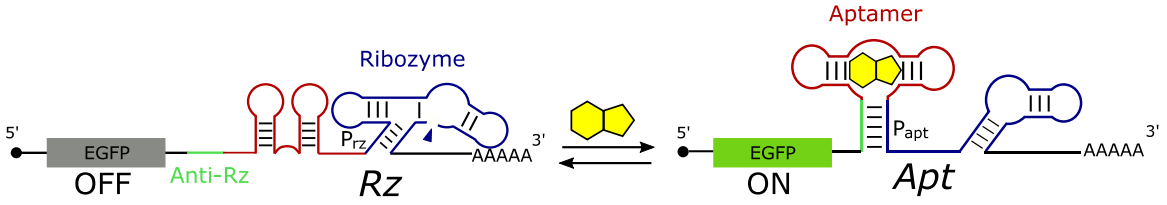

Figure 1. Schematic representation of the mammalian riboswitch based on the aptamer-ribozyme fusion architecture. The aptazyme preferentially forms the *Rz* structure which retains the active ribozyme fold in the absence of the aptamer ligand, resulting in mRNA cleavage. Aptamer-ligand binding disrupts the ribozyme fold (*Apt*) to prevent mRNA cleavage, and therefore allows protein translation.

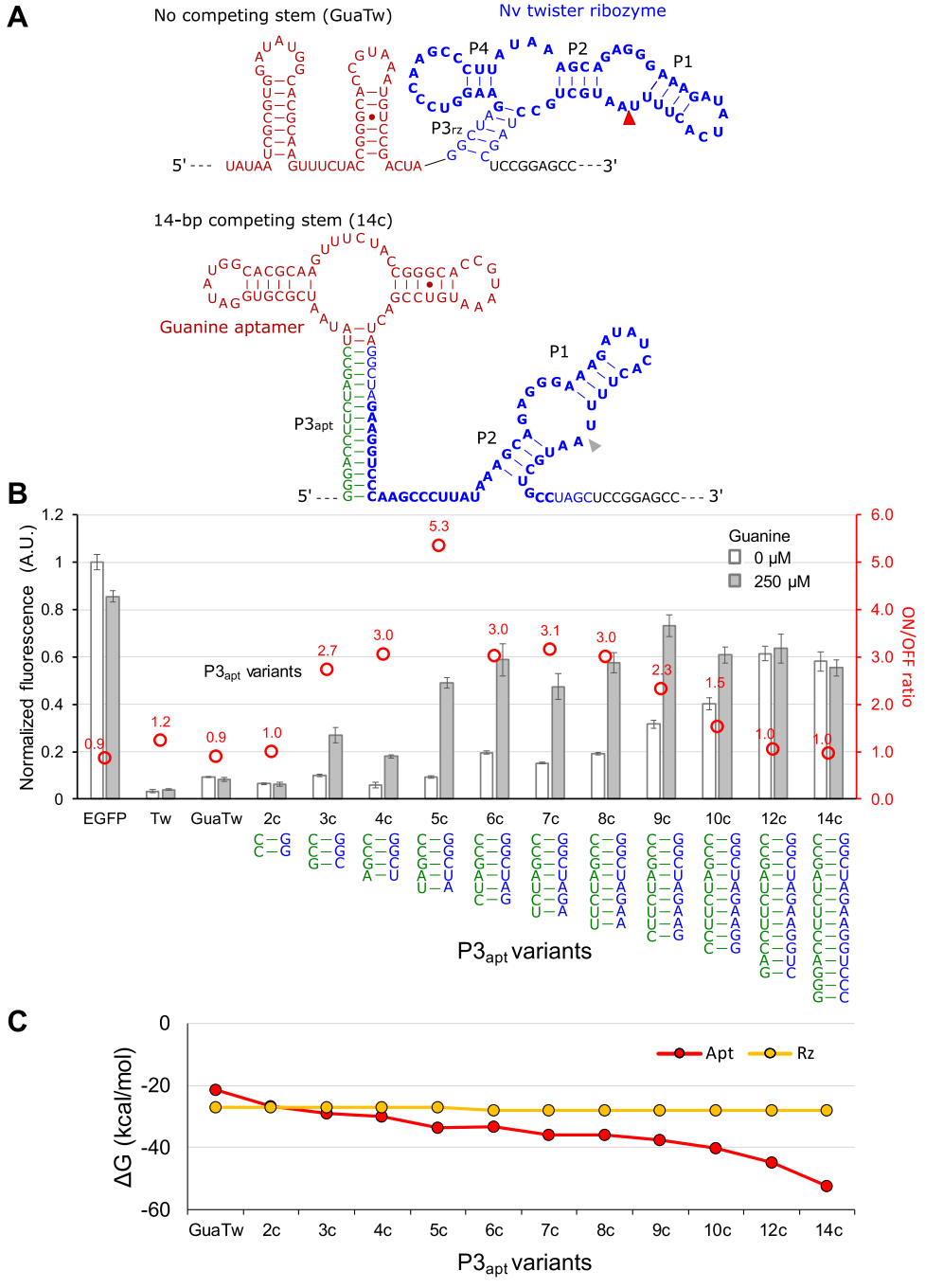

Figure 2. Optimization of $P3_{apt}$ size in the aptazyme architecture. (A) Predicted secondary structures of GuaTw (no upstream complementary bases) and 14c (14-base upstream complementary bases) aptazyme candidates. Red arrowhead indicates the cleavage site. (B) Normalized EGFP expression levels of the riboswitch variants in the absence and presence (250 μM) of guanine. EGFP: empty vector with no aptazyme. The data are averages of 3 replicate samples and the error bars represent SD. (C) Gibbs free energies (ΔG) of *Apt* and *Rz* structures calculated by Mfold. The structures were constrained to either *Apt*- or *Rz*-like folds by entering the constraint information provided in Table S1.

DOI: 10.1021/acssynbio.9b00371
ACS Synth. Biol. 2020, 9, 19−25

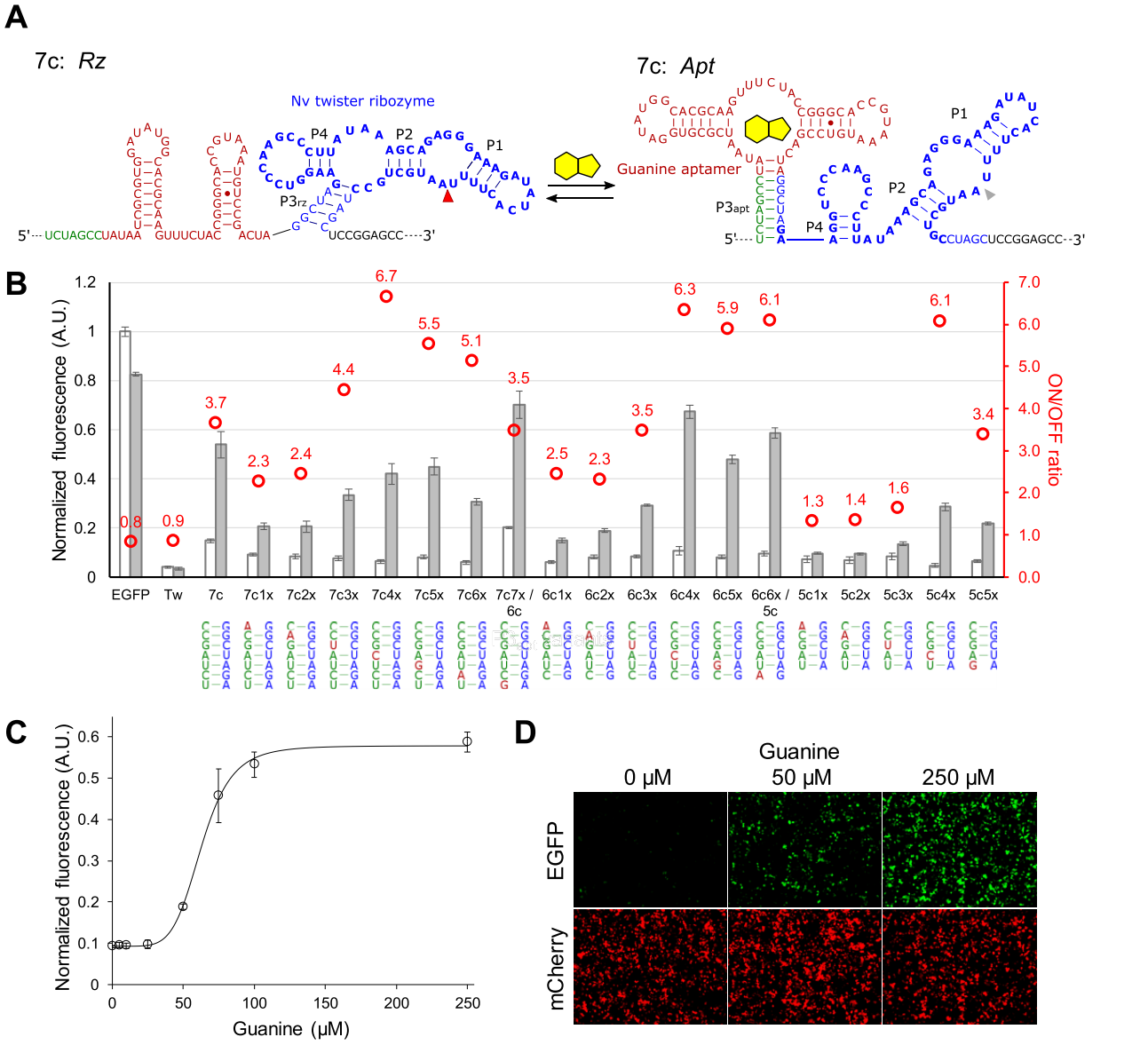

Figure 3. Optimization of $P3_{apt}$ stability in the aptazyme architecture by introducing mismatches. (A) Representative *Apt* and *Rz* structures illustrated for the 7c variant. (B) Normalized EGFP expression levels of the riboswitch variants in the absence and presence (250 μM) of guanine. EGFP: empty vector with no aptazyme. (C) Dose-dependent EGFP expression of 7c4x. The data are fitted to the Hill equation which is shown as the solid curve. (D) Fluorescence micrographs of the cells shown in (C). (B–C): The data are averages of 3 replicate samples, and the error bars represent SD.

expression (OFF). However, an optimal P_{apt} stability may shift the equilibrium of the aptazyme structures toward the *Apt* state in the presence of the aptamer ligand by selectively stabilizing the *Apt* structure, resulting in upregulation of gene expression (ON-switch). This aptazyme architecture was demonstrated using a guanine aptamer[21] and a pistol ribozyme[22] *in vitro*.[20] Unfortunately, however, the pistol ribozyme was not functional in mammalian cells; therefore, the tandem aptamer-ribozyme architecture was not implemented as a riboswitch.

In this work, we report successful design of guanine-activated riboswitches in mammalian cells based on this aptazyme architecture. Specifically, we used a guanine aptamer and a twister ribozyme[22] (first riboswitch application in mammalian cells), and systematically optimized the aptazyme design to yield mammalian ON-switches with ON/OFF ratios exceeding 6.0. This aptazyme design strategy expands the currently limited toolbox of RNA devices to control gene expression in mammalian cells.

RESULTS AND DISCUSSION

Twister ribozymes have been identified in many species of bacteria and eukaryotes,[23] and some variants have been shown to function efficiently in heterologous hosts. Felletti *et al.* used a twister ribozyme identified in the environmental DNAs to design synthetic riboswitches in *Escherichia coli* and *Saccharomyces cerevisiae*.[24] More recently, Litke and Jaffrey used a twister ribozyme from *Nematostella vectensis* to generate circular RNAs in mammalian cells.[25] Consequently, we also used the twister ribozyme from *N. vectensis* (simply referred to as Tw in this article) to design mammalian riboswitches.

We first confirmed the ribozyme activity in HEK293 cells by inserting Tw in the 3′ UTR of EGFP mRNA. The plasmid

DOI: 10.1021/acssynbio.9b00371
ACS Synth. Biol. 2020, 9, 19–25

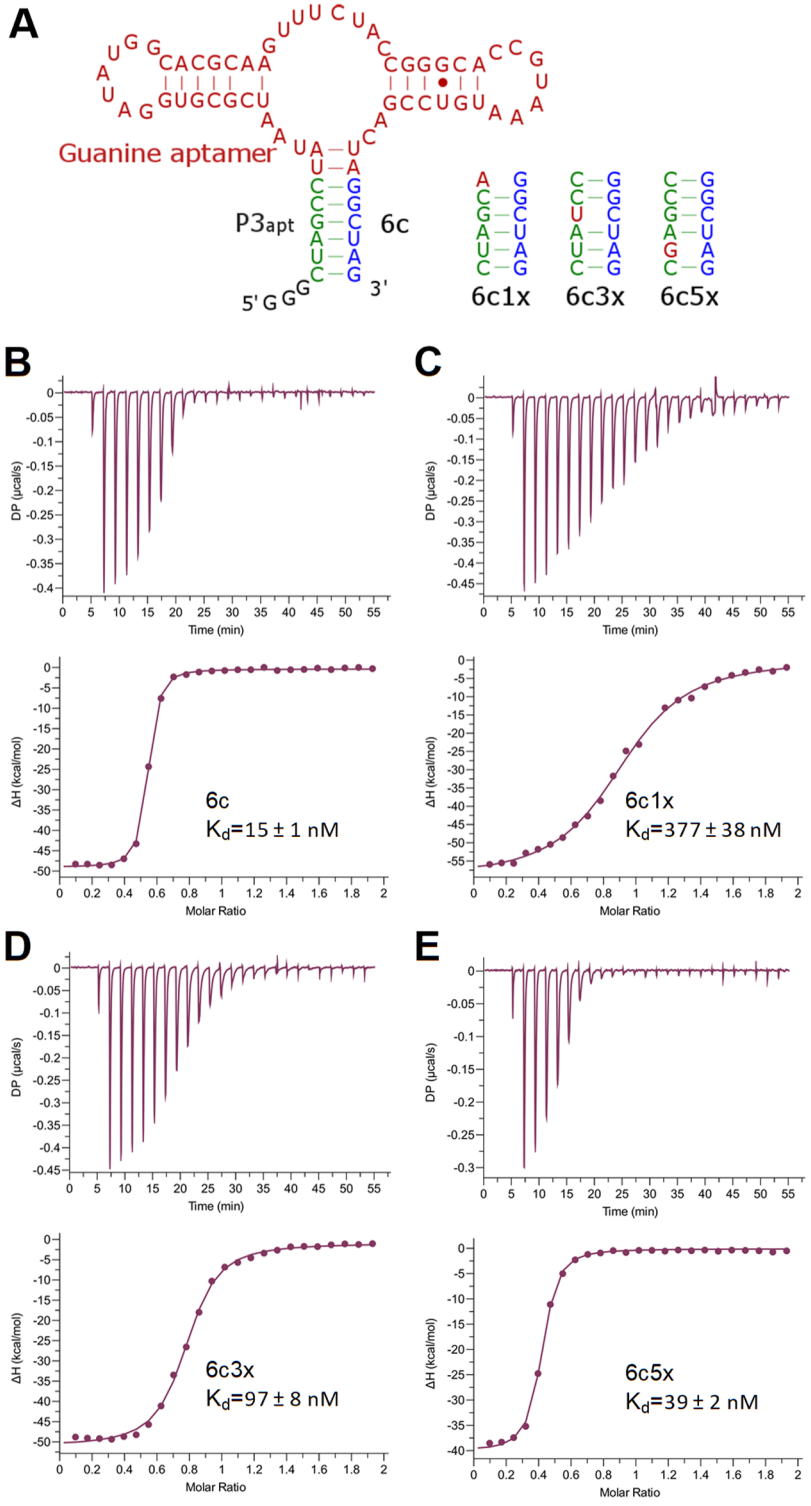

Figure 4. Effect of the mismatch position in the base stem of the guanine aptamer on K_d. (A) Stem variants of the aptamer studied by ITC. ITC results of the variants (B) 6c, (C) 6c1x, (D) 6c3x, and (E) 6c5x. Additional thermodynamic parameters obtained are provided in Table S2. The observations of binding stoichiometry (N) values lower than 1.0 have been reported for the guanine and other aptamers, probably due to the formation of nonfunctional complexes or misfolding.[27,28]

encoding the ribozyme-embedded EGFP and another plasmid constitutively expressing mCherry (used to normalize for transfection efficiency) were cotransfected into HEK293 cells, and cellular fluorescence was measured after 48 h. Expression of the Tw-embedded EGFP was suppressed by 96% compared to the control plasmid without ribozyme (Figure 2B), indicating fast self-cleavage of Tw in mammalian cells. Next, we inserted the core guanine aptamer sequence (Gua) directly upstream of Tw to produce GuaTw (Figure 2A). Fusion of Gua does not significantly interfere with the ribozyme activity of Tw as observed in the low EGFP fluorescence of the GuaTw-containing construct (Figure 2B).

DOI: 10.1021/acssynbio.9b00371
ACS Synth. Biol. 2020, 9, 19−25

We then extended the base stem of the guanine aptamer ($P3_{apt}$) which directly competes with the P3 stem of the ribozyme ($P3_{rz}$) (Figure 2A). On the basis of our previous work,[20] we envisioned that stabilization of $P3_{apt}$ would result in increased EGFP fluorescence due to the disruption of the competing $P3_{rz}$. As shown in Figure 2B, increasing the number of bases in $P3_{apt}$ that are complementary to Tw from 2 (2c) to 14 (14c) resulted in a gradual increase in EGFP fluorescence up to 12c where the EGFP level reaches a plateau. The same trend was observed in the presence of 250 μM guanine; however, EGFP expression mostly leveled off at 5c (Figure 2B). Consequently, the constructs 4c-8c functioned as guanine-activated riboswitches with ON/OFF ratios of approximately 3 or more.

Inactivation of Tw[23] in 14c (i14c) reduced the EGFP expression level relative to the empty vector by ∼27% (Figure S1), suggesting that the insertion of the sequence elements (ribozyme and aptamer) in the 3′UTR negatively affects the basal expression level in the absence of ribozyme cleavage. The EGFP expression level of 14c was ∼73% of that of i14c indicating that the $P3_{apt}$ in 14c mostly, although not completely, inhibits the ribozyme activity (Figure S1).

The results are consistent with our mechanistic hypothesis. When $P3_{apt}$ is weak (2c-4c), the aptazyme mostly adopts the *Rz* structure (Figure 1, left); therefore, the ribozyme is active and EGFP is downregulated. When $P3_{apt}$ is strong (12c and 14c), the aptazyme is biased toward the *Apt* structure (Figure 1, right), resulting in high EGFP expression. Intermediate stability of $P3_{apt}$, however, makes the relative stabilities of *Rz* and *Apt* structures dependent on the presence of guanine bound to the aptamer. Specifically, aptamer-guanine binding stabilizes the *Apt* structure relative to the *Rz* structure, therefore activating EGFP expression. The predicted free energy values of folding (ΔG)[26] of the *Apt* and *Rz* forms for the aptazymes indicate that while the *Rz* stability is unaffected by the number of upstream complementary bases (anti-Rz), the *Apt* structure stabilizes as the number of complementary bases increases (Figure 2C). We observed a sigmoidal relationship between EGFP expression and the energy difference of *Rz* and *Apt* structures ($\Delta G_{rz} - \Delta G_{apt}$) (Figure S2). Consistent with the assumption that guanine binding shifts the equilibrium toward *Apt*, the increase in EGFP expression is observed at lower $\Delta G_{rz} - \Delta G_{apt}$ in the presence of guanine, resulting in a small window ($\Delta G_{rz} - \Delta G_{apt}$ = ∼5−10 kcal/mol) in which the switching is observed. Consequently, adjusting the relative stability of $P3_{rz}$ and $P3_{apt}$ appears to be a viable strategy for optimizing the riboswitch performance.

Simply by changing the number of complementary bases to Tw in $P3_{apt}$, 5c, 6c, and 7c show respectable ON/OFF ratio of 3.0 to 5.3 (Figure 2B). We sought to further improve the riboswitch performance by lowering the OFF level in the absence of guanine. One way to achieve this is to destabilize $P3_{apt}$ relative to $P3_{rz}$ by introducing a mismatch in $P3_{apt}$ while keeping $P3_{rz}$ constant (Figure 3). Such a mutation would be expected to shift the equilibrium in favor of the *Rz* structure, and therefore to lower the EGFP expression level in the absence of guanine. By systematically introducing a mismatch within the $P3_{apt}$ stems of 5c, 6c, and 7c, we indeed observed reduction of the OFF levels in all variants (Figure 3B). Lower OFF levels of several variants contributed to the improved ON/OFF ratios with 4 variants displaying ON/OFF ratios greater than 6.0. The dose-dependent response of the variant 7c4x which showed an ON/OFF ratio of 6.7 was analyzed (Figure 3C,D). The riboswitch showed an EC_{50} of 63 μM which is comparable to that of the OFF-switch GuaM8HDVRz previously reported.[15]

A notable observation in Figure 3B is that the OFF level in the absence of guanine is largely unaffected by the position of the mismatch within $P3_{apt}$, but the ON level in the presence of guanine generally increases as the mismatch is located further away from the aptamer. The stability of the *Apt* structure in the absence of guanine, therefore, the OFF level, is expected to be mostly unaffected by the position of a mismatch within $P3_{apt}$. However, the stability of the *Apt* structure in the presence of guanine is affected by proximity of the mismatch within $P3_{apt}$ to the aptamer. A mismatch close to the guanine aptamer is more detrimental to guanine binding compared to a mismatch further away. Consequently, the riboswitch ON levels in the presence of guanine are lower when the mismatches are located closer to the aptamer (Figure 3B). This hypothesis was confirmed by measuring the dissociation constants (K_d) of guanine aptamers with and without a mismatch within the base stem (Figure 4). A mismatch proximal to the aptamer (6c1x) increased the K_d by 25-fold over the aptamer without a mismatch (6c). The K_d was 6.5-fold higher for 6c3x and 2.6-fold higher for 6c5x, consistent with the observations.

These observations are somewhat reminiscent of those by Zhong *et al.*,[12] who developed a scoring function to optimize the stability of the stem that connects an aptamer and a hammerhead ribozyme to optimize ligand-activated aptazymes that function as OFF-switches in mammalian cells. One of the key elements of their scoring function was to weigh the contributions of the base pairs closer to the ribozyme more than those further away. While the ribozyme architectures and the mode of the switches are different, the results underscore the importance of local stability within aptamer-ribozyme communication modules for the riboswitch performance.

Our results suggest that not only the relative stability of *Apt* and *Rz* structures, but also the subtle local stability within the stem structures influences the switch performance. While we focused on $P3_{apt}$ for optimization, fine-tuning the stability of $P3_{rz}$ may also prove to be a productive strategy. It should be noted, however, that while destabilization of $P3_{rz}$ would likely increase the ON level, it may also increase the OFF level by destabilizing the ribozyme structure. Again, the local stability within $P3_{rz}$ may affect the overall switch characteristics. Furthermore, mutations other than a mismatch, for example, introduction of a G-U wobble pair or a bulge (insertion), may also be worth testing. Consequently, more systematic and high-throughput screening of a larger set of mutants[19,29] guided by the structure−function relationship insights gained from this work may lead to further improvement of the riboswitch performance.

Although aptazyme-based riboswitches are the most frequently reported synthetic riboswitches in mammalian cells, only a handful of ON-switches have been reported. Furthermore, all of the existing ON-switches are based on inserting an aptamer in one of the stem-loops in a hammerhead ribozyme.[6,16−18] For example, the Suess group engineered an ON-switch by inserting the tetracycline aptamer in the P1 stem of a hammerhead ribozyme.[18] In that design, the nucleotides involved in the loop−loop interaction crucial for ribozyme activity were sequestered upon ligand binding. One of the variants K19 yielded a good ON/OFF ratio (8.7). Other existing aptazyme-based ON-switches have displayed

DOI: 10.1021/acssynbio.9b00371
ACS Synth. Biol. 2020, 9, 19−25

more modest ON/OFF ratios. The Hartig group recently demonstrated the modularity of the K19 riboswitch by changing the tetracycline aptamer to guanine aptamer resulting in a lower ON/OFF ratio of 4.0.[16] Similarly, the Smolke group has reported a theophylline activated riboswitch with the aptamer inserted within the P2 stem of a hammerhead ribozyme that shows an ON/OFF ratio of 3.1 in transiently transfected BHK cells.[7]

Even including the reported OFF-switches, the variety of aptamers, ribozymes, and aptazyme architectures used in mammalian riboswitches remains rather limited. Only two ribozyme classes (hammerhead and HDV ribozymes) have been used, and in all cases, an aptamer was inserted in a stem or a loop region within the ribozyme scaffold. To our knowledge, our work represents the first application of a twister ribozyme to regulate gene expression in mammalian cells. Additionally, the tandem aptamer-ribozyme architecture was demonstrated to function in living cells for the first time, yielding mammalian riboswitches with an ON/OFF ratio up to 6.7 through semirational and systematic fine-tuning of the P_{apt} stability. The new architecture expands the available RNA elements and design strategies for mammalian riboswitches.

Future goals include extension of the riboswitch architecture to other aptamers and ribozyme scaffolds, and optimization of the design strategy by identifying additional key sequence elements that affect riboswitch performance.

METHODS

Riboswitch Plasmid Preparation. All plasmids were constructed by standard recombinant DNA techniques and sequence verified by Sanger sequencing. The EGFP-aptazyme constructs were derived from pEGFP-N1-BspEI (Figure S3, Supporting Information, Appendix). The inserted riboswitch sequences are listed in Table S3. Plasmids used for transfection were purified using Zyppy Plasmid Miniprep kit (Zymo Research).

HEK293 Cell Culture and Transfection. HEK293 cells were cultured in Dulbecco's modified Eagle's medium (DMEM) supplemented with 10% heat-inactivated FBS (Gibco) containing 2 mM L-glutamine and 100 units/mL of penicillin-streptomycin (DMEM-FBS). Cells were kept in a 37°C incubator with 5% CO_2 and passaged regularly upon reaching 90% confluency. Approximately 20 h prior to transfection, the cells were trypsinized, diluted to ~2.7×10^5 cells/mL and 100 μL/well were seeded onto a 96-well plate. Cells in each well were cotransfected with 100 ng of the EGFP-aptazyme plasmid and 20 ng of pCMV-mCherry (transfection control) using 0.3 μL of *Trans*IT-293 Transfection Reagent (Mirus) according to the manufacturer's instructions. Five hours after transfection, the medium in each well was replaced with fresh medium with (250 μM) or without guanine. Guanine was dissolved at 25 mM in 0.2 M NaOH which was diluted by 100-fold in DMEM-FBS. The same volume of 0.2 M NaOH solution was diluted in DMEM-FBS for the medium without guanine. Forty-eight hours after transfection, the medium in each well was replaced with 100 μL of phosphate buffered saline (PBS), and fluorescence intensity was measured by Infinite M1000 PRO microplate reader (Tecan). Fluorescence intensity was measured at 484 nm excitation/510 nm emission/5 nm bandwidth for EGFP, and at 587 nm excitation/610 nm emission/10 nm bandwidth for mCherry. Background fluorescence measured using untransfected cells was subtracted from the EGFP and mCherry fluorescence values. Then, EGFP fluorescence was normalized by mCherry fluorescence to account for variations in transfection efficiency and cell counts. All reported values are averages of three replicate wells.

RNA Structure Prediction and Free Energy Calculation. For the free energy calculations (Figure 2C), aptazyme sequences were submitted to the Mfold Web Server's "RNA Folding Form".[26] The structure was constrained to either the *Apt* or *Rz* structure by forcing appropriate base pairs. The "constraint information" parameters used are listed in Table S1.

ITC Measurements. Guanine (Sigma-Aldrich) was dissolved in 1 N HCl/ethyl acetate solution and incubated at room temperature for few minutes. The solvent was removed by evaporation and the pellet was suspended in *n*-hexane. The solvent was removed again by evaporation to obtain guanine hydrochloride. Saturated solution of guanine hydrochloride was prepared in water and filtered through a 0.2 μm syringe filter (Merck-Millipore). The concentration was determined by absorbance using the reported molar extinction coefficient (ε_{248} = 11 400 cm^{-1} M^{-1}).[30] For titration experiments, 70.4 μM guanine solution was prepared in ITC buffer (10 mM HEPES-KOH, pH 7.5, 140 mM KCl, 10 mM NaCl, 1 mM $MgCl_2$).

Template DNAs for *in vitro* transcription were prepared by primer extension using Q5 High-Fidelity DNA Polymerase (NEB). Sequences of the oligo DNAs used are shown in Table S4. The resulting products were size-purified from agarose gel using a DNA purification kit (Zymoclean Gel DNA Recovery kit, Zymo Research). RNA aptamers were prepared using HiScribe T7 High Yield RNA Synthesis Kit (New England Biolabs) according to the manufacturer's instructions. The transcription products (100 μL) were treated with 2 U TURBO DNase (Thermo Fisher Scientific) at 37 °C for 1 h. The RNAs were precipitated with ammonium acetate and ethanol, and then dissolved in water. The solutions were further extracted with phenol-chloroform and ethanol precipitated. The RNAs were separated by denaturing polyacrylamide gel and extracted from the gel with TE buffer (10 mM Tris-HCl, pH 7.0, 0.1 mM EDTA-Na). The eluents were filtered through a 0.45 μm syringe filter. The gel-purified RNA solutions were concentrated, and the buffer was exchanged to water using an ultrafiltration device (Amicon Ultra 0.5 mL filter, 3 kDa cutoff, Merck-Millipore). RNA concentrations were determined by absorbance (A_{260}) according to OligoCalc.[31] For the titration experiments, 7.5 μM RNA solutions were prepared in the ITC buffer. RNAs were denatured at 65 °C for 3 min and then incubated at room temperature before measurement.

ITC experiments were performed as described previously with some modifications.[27] The titrations were performed at 37 °C using MicroCal PEAQ-ITC (Malvern). Injection parameters were as follows: initial 300 s delay, single 0.4 μL injection, and 24 serial injections of 1.5 μL at intervals of 120 s. Stirring speed and reference power were set to 700 rpm and 4.5 μcal s^{-1}, respectively. Raw data were analyzed with MicroCal PEAQ-ITC analysis software ver. 1.0.0.1259 (Malvern) depending on one-site binding model. Background signals (guanine hydrochloride was titrated against the buffer) were subtracted from the data. Measurements were repeated twice to ensure reproducibility.

DOI: 10.1021/acssynbio.9b00371
ACS Synth. Biol. 2020, 9, 19−25

■ ASSOCIATED CONTENT

Supporting Information

The Supporting Information is available free of charge at https://pubs.acs.org/doi/10.1021/acssynbio.9b00371.

DNA sequences of the riboswitch-coding sequences and the plasmid vector; Parameters used for free energy calculations; Thermodynamic parameters obtained in ITC experiments; Oligonucleotides used to synthesize guanine aptamer variants for ITC measurements (PDF)

■ AUTHOR INFORMATION

Corresponding Author

*E-mail: yohei.yokobayashi@oist.jp.

ORCID

Keisuke Fukunaga: 0000-0002-4259-4359

Yohei Yokobayashi: 0000-0002-2417-1934

Author Contributions

Y.Y. coordinated the project. K.M. designed and performed all experiments except ITC measurements. K.F. designed and performed the ITC experiments. All authors contributed to writing and editing of the manuscript.

Notes

The authors declare no competing financial interest.

■ ACKNOWLEDGMENTS

The research was funded by Okinawa Institute of Science and Technology Graduate University and Japan Society for the Promotion of Science (JSPS) KAKENHI 19H02855.

■ REFERENCES

(1) Berens, C., Groher, F., and Suess, B. (2015) RNA aptamers as genetic control devices: the potential of riboswitches as synthetic elements for regulating gene expression. *Biotechnol. J. 10*, 246−257.

(2) Etzel, M., and Mörl, M. (2017) Synthetic Riboswitches: From Plug and Pray toward Plug and Play. *Biochemistry 56*, 1181−1198.

(3) Hallberg, Z. F., Su, Y., Kitto, R. Z., and Hammond, M. C. (2017) Engineering and In Vivo Applications of Riboswitches. *Annu. Rev. Biochem. 86*, 515−539.

(4) Ausländer, S., and Fussenegger, M. (2017) Synthetic RNA-based switches for mammalian gene expression control. *Curr. Opin. Biotechnol. 48*, 54−60.

(5) Yokobayashi, Y. (2019) Aptamer-based and aptazyme-based riboswitches in mammalian cells. *Curr. Opin. Chem. Biol. 52*, 72−78.

(6) Chen, Y. Y., Jensen, M. C., and Smolke, C. D. (2010) Genetic control of mammalian T-cell proliferation with synthetic RNA regulatory systems. *Proc. Natl. Acad. Sci. U. S. A. 107*, 8531−8536.

(7) Bell, C. L., Yu, D., Smolke, C. D., Geall, A. J., Beard, C. W., and Mason, P. W. (2015) Control of alphavirus-based gene expression using engineered riboswitches. *Virology 483*, 302−311.

(8) Ketzer, P., Kaufmann, J. K., Engelhardt, S., Bossow, S., von Kalle, C., Hartig, J. S., Ungerechts, G., and Nettelbeck, D. M. (2014) Artificial riboswitches for gene expression and replication control of DNA and RNA viruses. *Proc. Natl. Acad. Sci. U. S. A. 111*, E554−562.

(9) Reid, C. A., Nettesheim, E. R., Connor, T. B., and Lipinski, D. M. (2018) Development of an inducible anti-VEGF rAAV gene therapy strategy for the treatment of wet AMD. *Sci. Rep. 8*, 11763.

(10) Strobel, B., Klauser, B., Hartig, J. S., Lamla, T., Gantner, F., and Kreuz, S. (2015) Riboswitch-mediated Attenuation of Transgene Cytotoxicity Increases Adeno-associated Virus Vector Yields in HEK-293 Cells. *Mol. Ther. 23*, 1582−1591.

(11) Takahashi, K., and Yokobayashi, Y. (2019) Reversible Gene Regulation in Mammalian Cells Using Riboswitch-Engineered Vesicular Stomatitis Virus Vector. *ACS Synth. Biol. 8*, 1976−1982.

(12) Zhong, G., Wang, H., Bailey, C. C., Gao, G., and Farzan, M. (2016) Rational design of aptazyme riboswitches for efficient control of gene expression in mammalian cells. *eLife 5*, No. e18858.

(13) Ausländer, S., Ketzer, P., and Hartig, J. S. (2010) A ligand-dependent hammerhead ribozyme switch for controlling mammalian gene expression. *Mol. BioSyst. 6*, 807−814.

(14) Nomura, Y., Kumar, D., and Yokobayashi, Y. (2012) Synthetic mammalian riboswitches based on guanine aptazyme. *Chem. Commun. 48*, 7215−7217.

(15) Nomura, Y., Zhou, L., Miu, A., and Yokobayashi, Y. (2013) Controlling mammalian gene expression by allosteric hepatitis delta virus ribozymes. *ACS Synth. Biol. 2*, 684−689.

(16) Stifel, J., Spöring, M., and Hartig, J. S. (2019) Expanding the toolbox of synthetic riboswitches with guanine-dependent aptazymes. *Synth. Biol. 4*, ysy022.

(17) Kennedy, A. B., Vowles, J. V., d'Espaux, L., and Smolke, C. D. (2014) Protein-responsive ribozyme switches in eukaryotic cells. *Nucleic Acids Res. 42*, 12306−12321.

(18) Beilstein, K., Wittmann, A., Grez, M., and Suess, B. (2015) Conditional control of mammalian gene expression by tetracycline-dependent hammerhead ribozymes. *ACS Synth. Biol. 4*, 526−534.

(19) Xiang, J. S., Kaplan, M., Dykstra, P., Hinks, M., McKeague, M., and Smolke, C. D. (2019) Massively parallel RNA device engineering in mammalian cells with RNA-Seq. *Nat. Commun. 10*, 4327.

(20) Kobori, S., Takahashi, K., and Yokobayashi, Y. (2017) Deep Sequencing Analysis of Aptazyme Variants Based on a Pistol Ribozyme. *ACS Synth. Biol. 6*, 1283−1288.

(21) Mandal, M., Boese, B., Barrick, J. E., Winkler, W. C., and Breaker, R. R. (2003) Riboswitches control fundamental biochemical pathways in Bacillus subtilis and other bacteria. *Cell 113*, 577−586.

(22) Weinberg, Z., Kim, P. B., Chen, T. H., Li, S., Harris, K. A., Lunse, C. E., and Breaker, R. R. (2015) New classes of self-cleaving ribozymes revealed by comparative genomics analysis. *Nat. Chem. Biol. 11*, 606−610.

(23) Roth, A., Weinberg, Z., Chen, A. G., Kim, P. B., Ames, T. D., and Breaker, R. R. (2014) A widespread self-cleaving ribozyme class is revealed by bioinformatics. *Nat. Chem. Biol. 10*, 56−60.

(24) Felletti, M., Stifel, J., Wurmthaler, L. A., Geiger, S., and Hartig, J. S. (2016) Twister ribozymes as highly versatile expression platforms for artificial riboswitches. *Nat. Commun. 7*, 12834.

(25) Litke, J. L., and Jaffrey, S. R. (2019) Highly efficient expression of circular RNA aptamers in cells using autocatalytic transcripts. *Nat. Biotechnol. 37*, 667−675.

(26) Zuker, M. (2003) Mfold web server for nucleic acid folding and hybridization prediction. *Nucleic Acids Res. 31*, 3406−3415.

(27) Dwidar, M., Seike, Y., Kobori, S., Whitaker, C., Matsuura, T., and Yokobayashi, Y. (2019) Programmable Artificial Cells Using Histamine-Responsive Synthetic Riboswitch. *J. Am. Chem. Soc. 141*, 11103−11114.

(28) Chandra, V., Hannan, Z., Xu, H. Z., and Mandal, M. (2017) Single-molecule analysis reveals multi-state folding of a guanine riboswitch. *Nat. Chem. Biol. 13*, 194−201.

(29) Kobori, S., Nomura, Y., Miu, A., and Yokobayashi, Y. (2015) High-throughput assay and engineering of self-cleaving ribozymes by sequencing. *Nucleic Acids Res. 43*, e85.

(30) Windholz, M. (1976) *The Merck Index: An Encyclopedia of Chemicals and Drugs*, 9th ed., Merck, Rahway, NJ.

(31) Kibbe, W. A. (2007) OligoCalc: an online oligonucleotide properties calculator. *Nucleic Acids Res. 35*, W43−W46.

DOI: 10.1021/acssynbio.9b00371
ACS Synth. Biol. 2020, 9, 19−25